A synthetic glycerol assimilation pathway demonstrates biochemical constraints of cellular metabolism

Steffen N. Lindner[1], Selçuk Aslan[1], Alexandra Müller[1], Eugenia Hoffart[2], Patrick Behrens[1], Christian Edlich-Muth[1], Bastian Blombach[2,3] and Arren Bar-Even[1]

1 Max Planck Institute of Molecular Plant Physiology, Potsdam-Golm, Germany
2 Institute of Biochemical Engineering, University of Stuttgart, Germany
3 Microbial Biotechnology, TUM Campus Straubing for Biotechnology and Sustainability, Technical University of Munich, Straubing, Germany

The engineering of synthetic metabolic routes can provide valuable lessons on the roles of different biochemical constraints in shaping pathway activity. In this study, we designed and engineered a novel glycerol assimilation pathway in *Escherichia coli*. While the synthetic pathway was based only on well-characterized endogenous reactions, we were not able to establish robust growth using standard concentrations of glycerol. Long-term evolution failed to improve growth via the pathway, indicating that this limitation was not regulatory but rather relates to fundamental aspects of cellular metabolism. We show that the activity of the synthetic pathway is fully controlled by three key physicochemical constraints: thermodynamics, kinetics and metabolite toxicity. Overcoming a thermodynamic barrier at the beginning of the pathway requires high glycerol concentrations. A kinetic barrier leads to a Monod-like growth dependency on substrate concentration, but with a very high substrate saturation constant. Finally, the flat thermodynamic profile of the pathway enforces a pseudoequilibrium between glycerol and the reactive intermediate dihydroxyacetone, which inhibits growth when the feedstock concentration surpasses 1000 mM. Overall, this study serves to demonstrate the use of synthetic biology to elucidate key design principles of cellular metabolism.

Introduction

The structure of metabolic pathways reflects a complex interplay between different selection pressures and biochemical constraints. Even the canonical structure of central metabolism shows major variations that reflect changing constraints under different environmental conditions. To give just few examples, nonphosphorylating glycolysis represents an adaptation to very high temperatures, where the instability of phosphorylated sugars becomes a major constraint [1–3]; the Entner–Doudoroff pathway is preferred over (Embden–Meyerhof–Parnas) glycolysis for obligatory aerobic metabolism in which the rate of glycolysis is more important than its ATP yield [4]; the methylglyoxal bypass, converting dihydroxyacetone phosphate into the highly reactive compound methylglyoxal, is utilized when phosphate starvation constrains glycolytic flux [5,6]; and the use of pyruvate formate-lyase, supporting 50% increase in ATP yield during sugar fermentation, reflects adaptation to microaerobic and anaerobic conditions [7,8].

Yet, many of the constraints imposed on the structure and function of central metabolism are hard to

Abbreviations
DO, dissolved oxygen; F6PA, fructose 6-phosphate aldolase; F6P, fructose 6-phosphate; GAP, glyceraldehyde 3-phosphate; $\Delta_r G'^m$, reaction change in Gibbs energy under reactant concentration of 1 mM and a constant pH.

derive from natural pathways, as these have specifically evolved to overcome such constraints. For example most assimilation routes start with an irreversible reaction (e.g. phosphorylation) to provide a thermodynamic driving force; hence, using natural pathways to study how a weak thermodynamic driving force limits pathway activity is challenging. Engineering and testing synthetic pathways can address this limitation and provide important lessons about key biochemical constraints that shape metabolism. Here, we demonstrate this approach by establishing a synthetic glycerol assimilation pathway and characterizing how different factors dictate its function.

Two routes are known to support glycerol assimilation [9] (Fig. 1A). In the first, glycerol is phosphorylated and oxidized to dihydroxyacetone phosphate, using quinones as electron acceptors. In the second, glycerol is first oxidized, donating its electrons to NAD^+, and then phosphorylated, either by ATP or phosphoenolpyruvate, to give dihydroxyacetone phosphate. Yet, many other metabolic configurations can potentially support glycerol assimilation into central metabolism. It is not clear whether the natural pathways represent an optimal structure, and, if so, which constraints might limit the activity of alternative routes. To address this, we engineer a third alternative to the two canonical routes, based solely on known reactions (Fig. 1B): dihydroxyacetone, generated by the NAD-dependent oxidation of glycerol, is assimilated via the activity of fructose 6-phosphate aldolase (F6PA, encoded by the *fsaA* gene). The other reactant, glyceraldehyde 3-phosphate (GAP), is 'borrowed' by F6PA and then returned by the subsequent activity of 6-phosphofructose kinase and fructose bisphosphate aldolase (Fig. 1B). As for the natural routes, the net product is dihydroxyacetone phosphate from which all biomass building blocks can be derived.

While the enzymatic components of the synthetic pathway – which we term the fructose 6-phosphate aldolase pathway – are all metabolically characterized and can channel high flux by themselves, we show that the activity of the pathway as a whole is highly constrained. As long-term evolution fails to evolve high pathway activity, we deduce that this limitation is not regulatory but rather relates to fundamental aspects of cellular metabolism. Using a series of experiments, we show that the activity of the F6PA pathway is dictated by three physiochemical constraints: thermodynamics, kinetics and metabolite toxicity. The interplay between these constraints results in a unique growth phenotype, which sheds light on the biochemical logic of metabolic pathways. Specifically, a thermodynamic barrier at the pathway start necessitates high glycerol concentration to

enable growth. A kinetic barrier, which stems at least partially from the thermodynamic constraint, results in a Monod curve shifted towards high concentrations, where growth rate keeps increasing up to 700 mM glycerol. Finally, the flat thermodynamic profile of the pathway results in pseudoequilibrium between glycerol and the metabolic intermediate dihydroxyacetone, such that at glycerol concentrations > 1 M, the deleterious accumulation of this reactive metabolite inhibits growth.

Results

The activity of the F6PA-pathway is limited at standard concentrations of glycerol

We first tested whether the F6PA pathway can support growth on glycerol at the 'standard' (i.e. commonly used for laboratory-scale cultivation of *Escherichia coli*) concentration of 20 mM. We constructed an *E. coli* strain deleted in both glycerol kinase and dihydroxyacetone kinase ($\Delta glpK$ $\Delta dhaK$), which was thus incapable of assimilating glycerol via either of the natural routes. We tested whether overexpression of the native glycerol dehydrogenase (encoded by *gldA*) and fructose-6-phosphate aldolase (encoded by *fsaA*) could rescue growth on glycerol (Fig. 1B). However, as shown in Fig. 2A,B, we did not observe growth.

We therefore decided to reduce the selection pressure for glycerol assimilation via F6PA. For this aim, we deleted, within the $\Delta glpK$ $\Delta dhaK$ strain, the two isozymes of fructose bisphosphatase [10], resulting in a $\Delta glpK$ $\Delta dhaK$ Δfbp $\Delta glpX$ strain. This strain was expected to grow on glucose, but growth on pyruvate – or any other 'lower metabolism' carbon source – should not be possible, since gluconeogenesis is blocked at the level of fructose 1,6-bisphosphate and the cell cannot synthesize essential sugar phosphates: fructose 6-phosphate (F6P), glucose 6-phosphate, erythrose 4-phosphate and ribose 5-phosphate. Indeed, as shown in Fig. 2C, growth of the $\Delta glpK$ $\Delta dhaK$ Δfbp $\Delta glpX$ strain was possible on glucose but not on pyruvate.

We expected that the overexpression of *gldA* and *fsaA* in the $\Delta glpK$ $\Delta dhaK$ Δfbp $\Delta glpX$ strain would enable growth on pyruvate and glycerol: pyruvate metabolism provides GAP while glycerol oxidation provides dihydroxyacetone, which together can be condensed, by F6PA, to give F6P. The pentose phosphate pathway can subsequently metabolize F6P to provide all required sugar phosphates (Fig. 3A). As expected, only upon overexpression of *gldA* and *fsaA* did we observe growth on 20 mM pyruvate and 20 mM glycerol (Fig. 2D), where glycerol alone resulted in
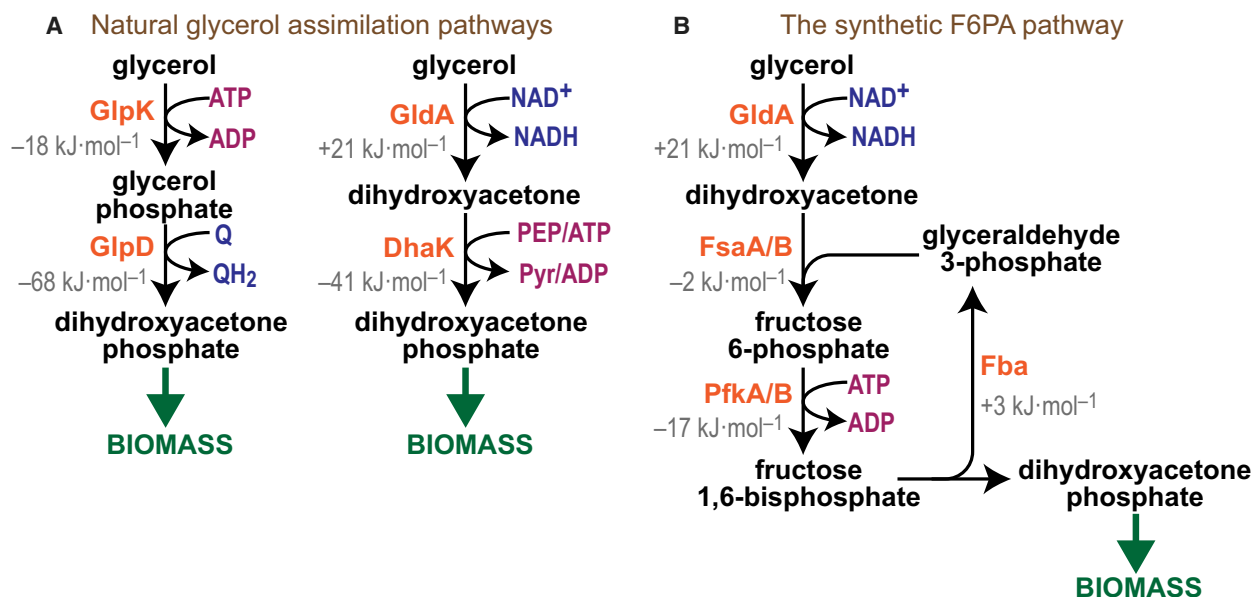
A Natural glycerol assimilation pathways

glycerol

GlpK — ATP

−18 kJ·mol^{-1} — ADP

glycerol phosphate

GlpD — Q

−68 kJ·mol^{-1} — QH$_2$

dihydroxyacetone phosphate

BIOMASS

glycerol

GldA — NAD$^+$

+21 kJ·mol^{-1} — NADH

dihydroxyacetone

DhaK — PEP/ATP

−41 kJ·mol^{-1} — Pyr/ADP

dihydroxyacetone phosphate

BIOMASS

B The synthetic F6PA pathway

glycerol

GldA — NAD$^+$

+21 kJ·mol^{-1} — NADH

dihydroxyacetone

FsaA/B — **glyceraldehyde 3-phosphate**

−2 kJ·mol^{-1}

fructose 6-phosphate

PfkA/B — ATP

−17 kJ·mol^{-1} — ADP

Fba
+3 kJ·mol^{-1}

fructose 1,6-bisphosphate → **dihydroxyacetone phosphate**

BIOMASS

Fig. 1. Metabolic structure of different glycerol assimilation pathways. (A) Natural glycerol assimilation pathways. (B) The proposed, synthetic fructose 6-phosphate aldolase (F6PA) pathway. Reaction change in Gibbs energy at reactant concentration of 1 mM ($\Delta_r G'^m$) is shown in grey next to each reaction; values were calculated using eQuilibrator [11].

negligible growth only. Importantly, while *gldA* and *fsaA* are endogenous in *E. coli*, their native expression levels were too low to support growth: overexpression of *gldA* alone or *fsaA* alone did not support growth on pyruvate and glycerol.

To confirm that the growth on pyruvate and glycerol follows the metabolic pattern we predicted, we cultivated the strain on completely ^{13}C-labelled glycerol and unlabelled pyruvate and measured the labelling pattern in different proteinogenic amino acids. As shown in Fig. 3B, both alanine and serine – which can be derived solely from pyruvate – are negligibly labelled, whereas histidine – two carbons of which are expected to be derived from glycerol (Fig. 3A) – is almost completely doubly labelled. These results demonstrate that the combined activities of GldA and F6PA can support flux in the desired assimilatory direction. (We note the different labelling of the amino acids within a WT strain, where the labelling of serine and alanine indicates that glycerol is oxidized by glycolysis and the labelling of histidine indicates that it is mainly produced from glycerol.)

Long-term evolution fails to achieve growth on low concentration of glycerol via the F6PA pathway

At this point, we were wondering whether the F6PA pathway fails to support growth on glycerol as sole

carbon source due to regulatory limitations. For example low induction of the glycerol channel (GlpF, upregulated by glycerol 3-phosphate [9]) or inhibition of a downstream enzyme, such as phosphofructokinase, could potentially limit glycerol assimilation. We anticipated that a long-term continuous cultivation under selective conditions would optimize the regulatory network and therefore lead to the emergence of a strain capable of growing on glycerol as sole carbon source via the F6PA pathway. Towards this aim we cultivated the $\Delta glpK$ $\Delta dhaK$ Δfbp $\Delta glpX$ strain, overexpressing *gldA* and *fsaA*, in a chemostat mode with limiting amounts of pyruvate (5 mM) and nonlimiting amounts of glycerol (40 mM). At the end of each week, we took a sample from the culture and tried to cultivate it on glycerol as a sole carbon source. However, even after 75 days of evolution ($\approx$ 100 generations) we failed to see sustained growth on glycerol (Fig. 4). We then decided to reduce the level of pyruvate to 3 mM, and see whether the lower availability of pyruvate would assist in selecting for growth on glycerol. As shown in Fig. 4, upon reduction in pyruvate concentration, the OD within the bioreactor initially dropped, but regained its previous level after $\sim$ 1 month of further cultivation. Still, even after completing 120 days of chemostat cultivation ($\approx$ 160 generations), we were not able to isolate a strain capable of growing on glycerol as sole carbon source. This failure prompted us to think that the problem might not be regulatory, but rather fundamental, that is, related to basic
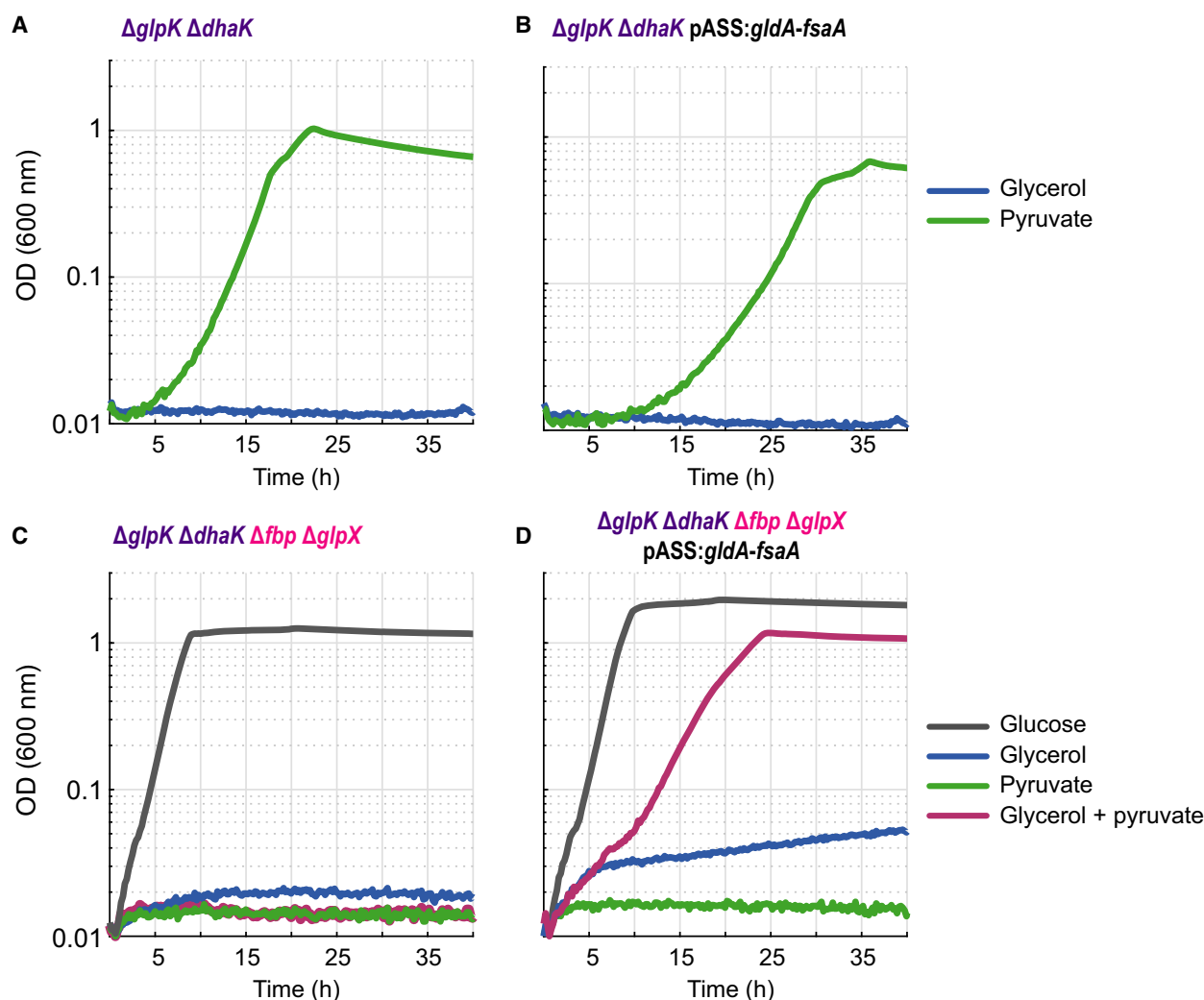
Fig. 2. Assimilation of standard concentration (20 mM) of glycerol. (A) A strain deleted in glycerol kinase (Δ*glpK*) and dihydroxyacetone kinase (Δ*dhaK*) loses its ability to growth on glycerol. (B) Overexpression of *gldA* and *fsaA* does not rescue growth on glycerol, despite providing a potential assimilation route via the F6PA pathway. (C, D) Further deletion of fructose bisphosphatase (Δ*fbp* Δ*glpX*) enabled growth on glycerol and pyruvate only when *gldA* and *fsaA* were overexpressed, indicating the activity of F6PA pathway as the sole route for the biosynthesis of essential phosphosugars such as fructose 6-phosphate, glucose 6-phosphate, erythrose 4-phosphate, and ribose 5-phosphate. Glucose was used as a positive control while pyruvate alone served as a negative control. All experiments were conducted in triplicates in 96-well plates; shown are the averages of the triplicates, which, in all cases, did not differ by more than 10%. Pyruvate concentration was 20 mM and glucose concentration was 10 mM.

properties of the process, and especially its thermodynamics and kinetics.

Unfavourable thermodynamics, poor kinetics and metabolite toxicity shape pathway activity

Oxidation of glycerol to dihydroxyacetone, using NAD as an electron acceptor, is unfavourable, having $\Delta_r G'^m \sim +20$ kJ·mol^{-1} at physiological pH 7.5 and ionic strength of 0.25 mM ($\Delta_r G'^m$ refers to change in Gibbs energy when all reactants are at a concentration of 1 mM) [11,12]. The following aldol condensation reaction has $\Delta_r G'^m \sim 0$, which does not help to resolve the thermodynamic bottleneck. If we assume that the concentration of GAP is ~ 30 μM (in equilibrium with that of dihydroxyacetone phosphate, ~ 300 μM [13]) and that [NAD]/[NADH] ~ 10 [13], then the concentration of F6P needs to be ~ 4 orders of magnitude lower than that of glycerol to enable assimilatory flux, i.e., achieve $\Delta_r G' < 0$. In other words, to maintain a reasonable cellular level of F6P, very high concentrations of glycerol are needed.
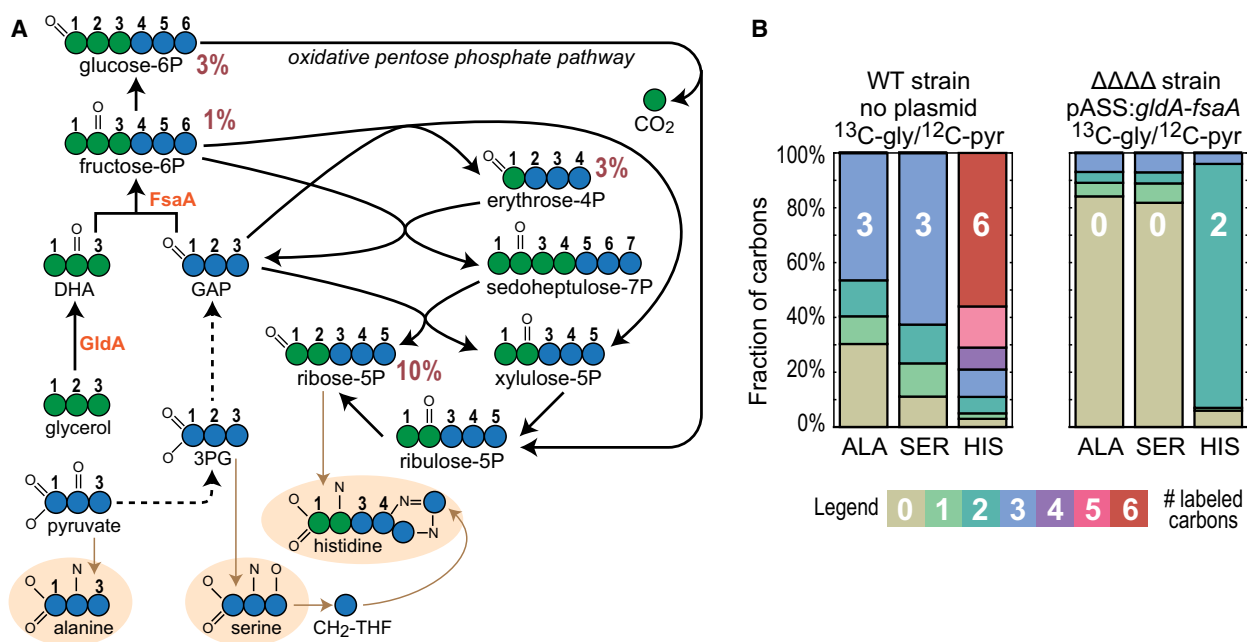
Fig. 3. Co-assimilation of pyruvate and glycerol via the F6PA pathway in a strain deleted in glycerol kinase, dihydroxyacetone kinase and fructose bisphosphatase. (A) Expected distribution of carbons molecules that originate from pyruvate and glycerol within phosphosugars and amino acids. Both the oxidative and nonoxidative pentose phosphate pathways are expected to result in ribose 5-phosphate in which two carbons originate from glycerol. (B) Labelling pattern of proteinogenic amino acids upon feeding with $^{13}C_3$-Glycerol. In the $\Delta glpK$ $\Delta dhaK$ Δfbp $\Delta glpX$ strain (marked with $\Delta\Delta\Delta\Delta$) overexpressing *gldA* and *fsaA*, alanine and serine are mostly unlabelled as they are derived from ^{12}C-pyruvate, while histidine, which originates for ribose 5-phosphate, harbours two carbons that originate from $^{13}C_3$-Glycerol.
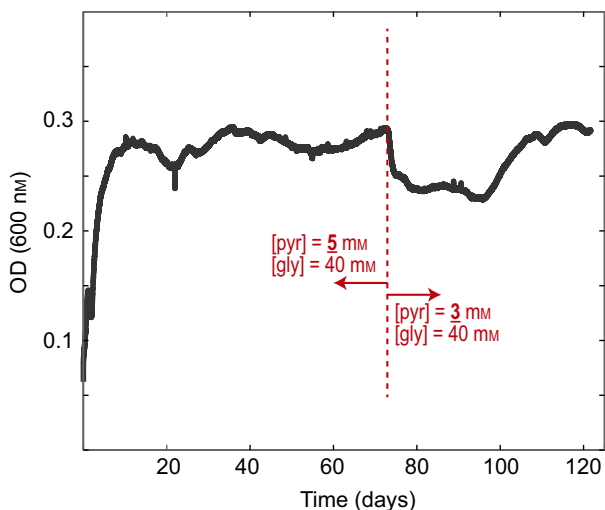

Fig. 4. Long-term chemostat cultivation of the $\Delta glpK$ $\Delta dhaK$ strain overexpressing *gldA* and *fsaA* on low concentrations of glycerol and pyruvate. Concentrations of glycerol and pyruvate were changed on day 75 as marked in the figure. Samples were taken every week but failed to show growth on 20 mM glycerol as a sole carbon source.

Therefore, we conducted a growth experiment with a higher concentration of glycerol. As shown in Fig. 5, 500 mM glycerol supported growth of the $\Delta glpK$
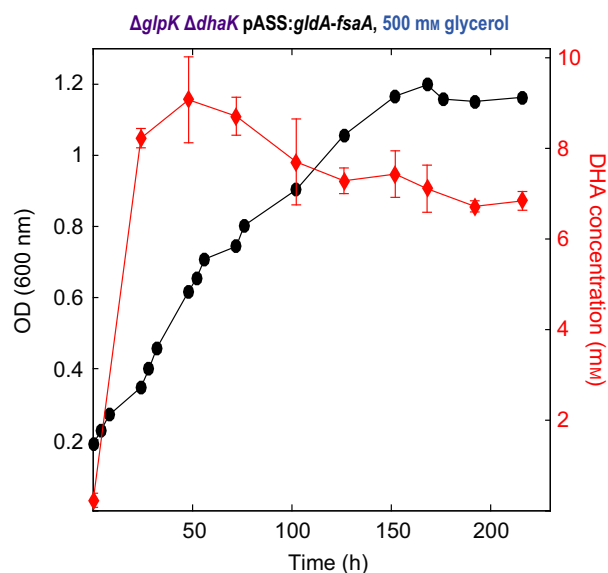

Fig. 5. Cultivation of the $\Delta glpK$ $\Delta dhaK$ strain overexpressing *gldA* and *fsaA* on 500 mM glycerol within a bioreactor (200 mL). Increase in OD is shown in black while accumulation of dihydroxyacetone is shown in red. Error bars correspond to standard deviation across three independent cultivations. No other byproduct was observed in the medium.
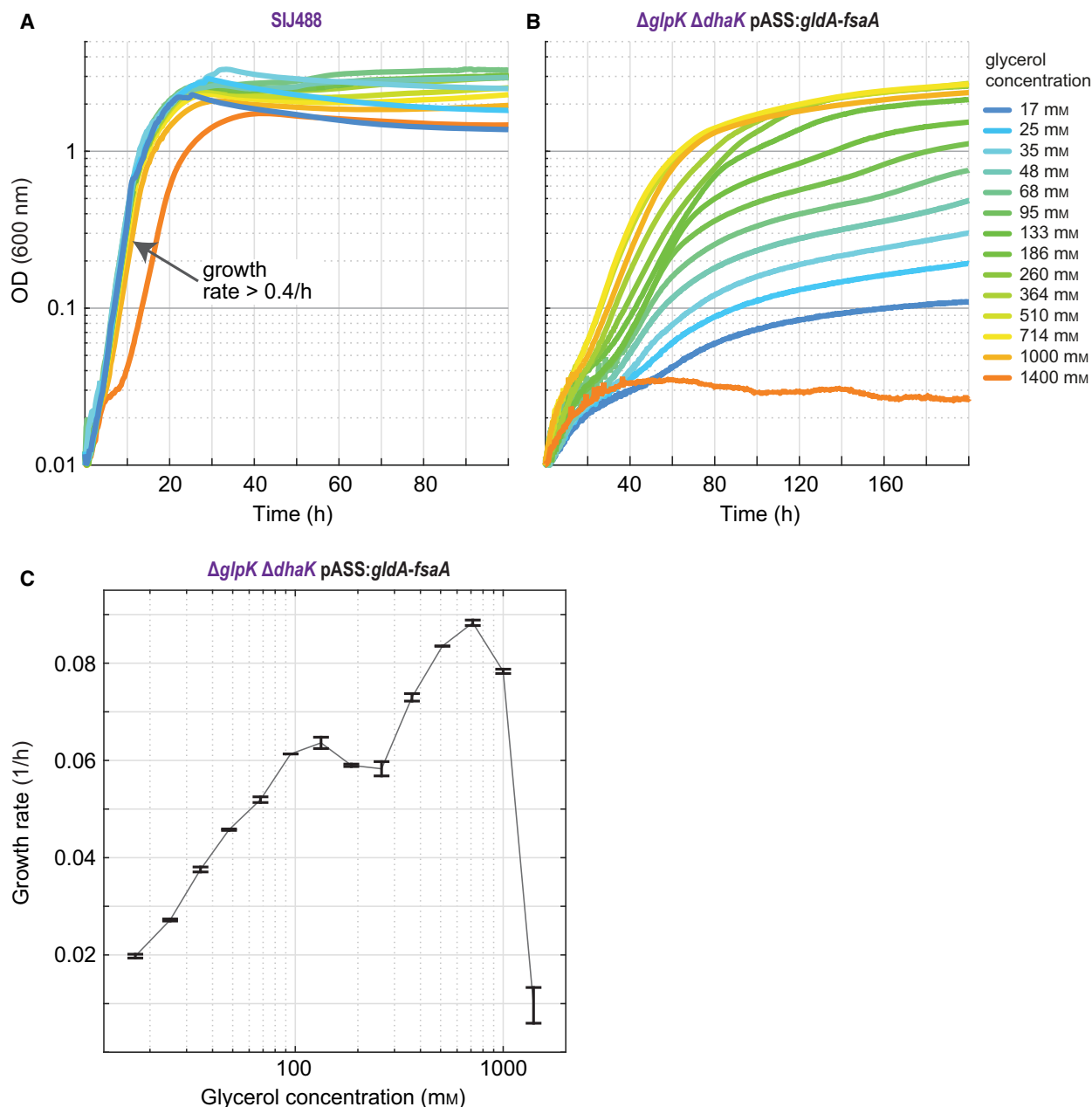
Fig. 6. Cultivation of the Δ*glpK* Δ*dhaK* strain overexpressing *gldA* and *fsaA* on different concentrations of glycerol. (A) Growth curves of *Escherichia coli* SIJ488 (WT). (B) Growth curves of Δ*glpK* Δ*dhaK* strain overexpressing *gldA* and *fsaA*. All experiments were conducted in triplicates in 96-well plates; shown are the averages of the triplicates, which, in all cases, did not differ by more than 10%. (C) Growth rates (1/h) of Δ*glpK* Δ*dhaK* strain overexpressing *gldA* and *fsaA* as function of glycerol concentrations. Error bars correspond to standard errors.

Δ*dhaK* strain overexpressing *gldA* and *fsaA* within a 200 mL bioreactor (overexpression of *gldA* alone or *fsaA* alone did not support growth). When we analysed the medium, we identified dihydroxyacetone which accumulated at the beginning of the fermentation and then remained rather constant throughout the growth phase. No other organic compound, besides

glycerol, could be detected in the medium (Methods). We confirmed that the increase in OD corresponds to cell growth, rather than a change in the absorption property of the medium, by measuring the biomass concentration at different OD values.

We wanted to confirm that growth on glycerol indeed takes place via the F6PA pathway as shown in
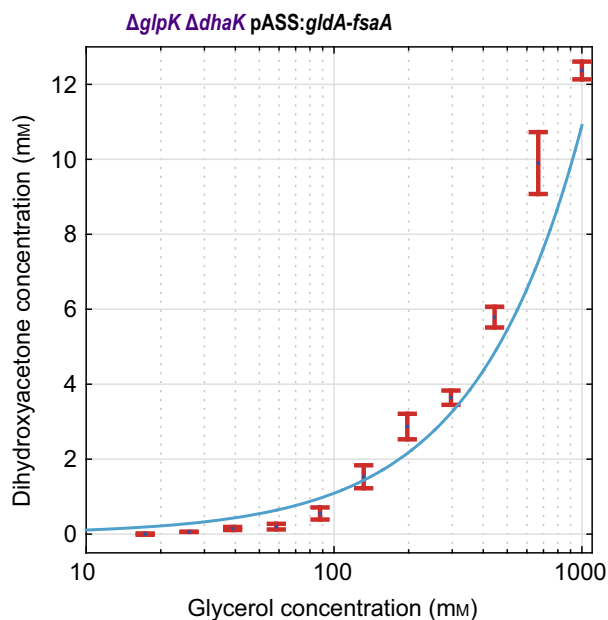
ΔglpK ΔdhaK pASS:gldA-fsaA

Fig. 7. Dihydroxyacetone concentration increases with increasing glycerol concentration, according to a thermodynamic trend. The concentration of dihydroxyacetone was measured in the supernatant of the Δ*glpK* Δ*dhaK* strain overexpressing *gldA* and *fsaA*. Error bars (in red) correspond to standard errors derived from three independent measurements. Light blue line corresponds to the predicted dihydroxyacetone concentration, assuming that it is in equilibrium with the concentration of glycerol. Thermodynamic calculations were based on the eQuilibrator website [11] and assuming that [NAD$^+$]/[NADH] = 50 [33].
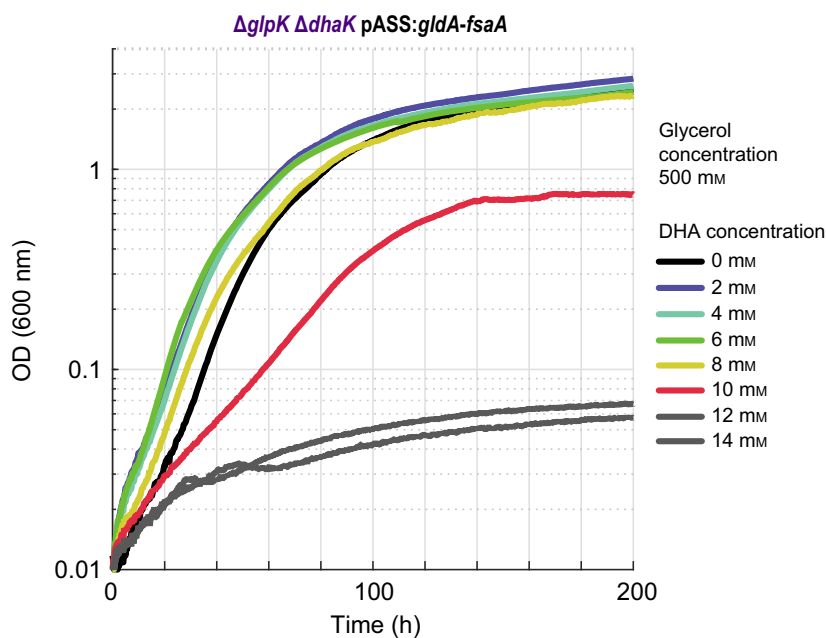
Fig. 1B such that fructose 6-phosphate is further metabolized by 6-phosphofructokinase – rather than by an alternative route (e.g. Entner–Doudoroff pathway). Towards this aim, we introduced further gene deletions to the Δ*glpK* Δ*dhaK* strain: we deleted either the two isozymes of 6-phosphofructokinase (Δ*pfkA* Δ*pfkB*) or glucose 6-phosphate dehydrogenase (Δ*zwf*, entry point of the Entner–Doudoroff pathway). We found that while the Δ*glpK* Δ*dhaK* Δ*pfkA* Δ*pfkB* strain (overexpressing *gldA* and *fsaA*) could not grow on glycerol (regardless of the concentration), the growth of the Δ*glpK* Δ*dhaK* Δ*zwf* strain was identical to that of the parent Δ*glpK* Δ*dhaK* strain. This indicates that F6P is indeed assimilated via its phosphorylation to fructose 1,6-bisphosphate and downstream glycolysis, rather than via the oxidative pentose phosphate pathway and/or the Entner–Doudoroff pathway.

Next, we asked how different concentrations of glycerol affect growth. While the growth rate of a WT strain remained high, above 0.4/h, at all glycerol concentrations (Fig. 6A), the growth rate of the engineered Δ*glpK* Δ*dhaK* strain (overexpressing *gldA* and *fsaA*) was strongly dependent on glycerol concentration (Fig. 6B). Similar to the classical Monod model [14], at 'low' glycerol concentrations there was a linear relationship between concentrations and growth rate (despite a small drop in growth rate at 200–300 mM glycerol). The observed Monod relationship, however, displayed a low maximal growth rate and a very high substrate saturation constant, indicating a

ΔglpK ΔdhaK pASS:gldA-fsaA

Fig. 8. Dihydroxyacetone toxicity for strain Δ*glpK* Δ*dhaK* overexpressing *gldA* and *fsaA*. The strain was cultivated on 500 mM glycerol, to which different concentrations of dihydroxyacetone were added. All experiments were conducted in triplicates in 96-well plates; shown are the averages of the triplicates, which, in all cases, did not differ by more than 10%.

strong kinetic bottleneck for glycerol assimilation (see Discussion).

At high glycerol concentrations, > 700 mм, growth started to slow and was effectively abolished at 1400 mм glycerol (Fig. 6C). We interpret this to indicate that dihydroxyacetone – the concentration of which is expected to be close to equilibrium with that of glycerol – has reached a toxic level. Indeed, dihydroxyacetone and its metabolic derivative methylglyoxal are well known to be highly reactive and to strongly inhibit cell growth [15–17].

To confirm that the growth collapse observed at high glycerol concentration relates to the accumulation of dihydroxyacetone, we measured the steady-state concentration of this reactive metabolite upon feeding the engineered strain with varying levels of glycerol. As shown in Fig. 7, we found that dihydroxyacetone concentrations increased with the concentration of glycerol, following the thermodynamically expected trend, which assumes a pseudoequilibrium of the two compounds (marked with a light blue line). At glycerol concentrations approaching 1000 mм, the concentration of dihydroxyacetone surpassed 10 mм. To confirm that such dihydroxyacetone concentration is indeed toxic, we added different levels of dihydroxyacetone to 500 mм glycerol (which otherwise supports growth). As shown in Fig. 8, growth of the engineered strain was abolished when the supplemented dihydroxyacetone exceeded a concentration of 10 mм. These experiments thus support our interpretation that growth at high glycerol concentrations become impossible due to the deleterious accumulation of dihydroxyacetone. We note that since the growth of a WT strain does not involve the production of dihydroxyacetone, this strain can tolerate high concentrations of glycerol.

Discussion

The synthetic F6PA pathway provides a unique opportunity to observe the interplay between different metabolic constraints, an opportunity rarely available with natural pathways evolved to overcome such barriers. Three key elements explain the observed growth via the F6PA pathway: thermodynamics, kinetics, and metabolite toxicity. As discussed above, the thermodynamic barrier of the F6PA pathway requires a high level of glycerol to support assimilatory flux while keeping the concentration of the key metabolic intermediate F6P at a physiologically relevant concentration. This explains why growth at a 'standard' concentration of 20 mм was unsuccessful without the addition of another carbon source, pyruvate, which substantially reduced the metabolic requirement of the

F6PA pathway and provided GAP to thermodynamically 'push' dihydroxyacetone assimilation. We note that the native glycerol assimilation pathway in which glycerol is also initially reduced to dihydroxyacetone using NAD as an acceptor (Fig. 1A) does not suffer from the same thermodynamic barrier since the subsequent reaction, dihydroxyacetone phosphorylation, is thermodynamically and kinetically favourable. Hence, the concentration of dihydroxyacetone is kept low enough as to enable glycerol oxidation to operate far from equilibrium .

Even at high glycerol concentrations, the observed growth via the synthetic F6PA pathway was rather unusual. Specifically, the growth generally corresponds to a Monod model, but with a low maximal growth rate and a very high substrate saturation constant [14,18,19]. We argue that these poor Monod parameters can be explained by the very harsh kinetic constraints that underlie the activity of the F6PA pathway. This kinetic constraint is directly related to the thermodynamic barrier: the overall unfavourable nature of the pathway indicates that it operates at a low energetic driving force, i.e., close to equilibrium, which substantially lowers flux [20,21]. On top of this main barrier, poor enzyme kinetics further lowers pathway rate. Specifically, while alcohol dehydrogenase enzymes, such as GldA, are characterized by a high k_{cat} in the carbonyl reduction direction, the Haldane relationship – linking the kinetics of a reaction in both directions to its thermodynamics [22] – dictates poor kinetics for glycerol oxidation. Moreover, the low affinity of F6PA towards dihydroxyacetone ($K_M \sim 32$ mм) and low cellular concentration of GAP further constrains the rate of F6P production. Finally, several of the enzymes downstream of F6P are characterized by a relatively low affinity – for example transaldolase with $K_M > 1$ mм for F6P [23] – such that their rate is expected to drop due to a low F6P concentration. The immense kinetic barrier that results from the combination of these factors accounts for the observed growth phenotype.

In contrast to the standard Monod model, however, growth on glycerol comes to an abrupt stop at high concentrations of glycerol (> 1000 mм). This is attributed to another key constraint – accumulation of a reactive intermediate, dihydroxyacetone in this case. As dihydroxyacetone lies at the centre of the thermodynamic and kinetic barriers, its concentration is close to equilibrium with that of the glycerol. This is not the case in the natural glycerol assimilation pathway in which glycerol is first oxidized to dihydroxyacetone. In the latter case, the downstream phosphorylation of dihydroxyacetone is highly favourable both thermodynamically and

kinetically, and thus expected to enable much lower steady-state concentration of dihydroxyacetone.

As a further confirmation of the accumulation of dihydroxyacetone via the activity of the F6PA pathway, we noticed that the growth medium became brownish during the growth experiments, indicative of a Maillard reaction between reactive dihydroxyacetone and amines [24]. Interestingly, we observed this brownish colouring also at concentrations of glycerol which were too high to support growth, indicating that the nongrowing cells were metabolically active and produced dihydroxyacetone at high levels.

While the F6PA pathway is most definitely inferior to its natural counterparts in assimilating glycerol, it represents a unique metabolic biosensor strain. Specifically, working within the linear regime of the Monod curve enables one to quantify the concentration of the feedstock compound by measuring the growth rate. Notably, this is a special case, as the linear regime associated with most carbon sources and metabolic pathways is limited to vanishingly low feedstock concentrations, such that microbial growth cannot be easily detected. As the linear regime associated with the F6PA pathway is shifted to high feedstock concentrations that support detectable growth, the strain can be easily used to analyse glycerol concentration within the medium.

To conclude, this study serves to demonstrate the capability of synthetic biology to illustrate principle physicochemical constraints *in vivo*. We showed that the F6PA pathway provides a valuable lesson regarding the interplay between three key aspects of metabolism – thermodynamics, kinetics, and reactivity. It is therefore evident that besides addressing societal challenges, synthetic biology offers effective tools to uncover the design principles and biochemical logic of cellular metabolism.

Materials and methods

Strains and plasmids

All strains used in this study are listed in Table 1. *E. coli* strain SIJ488 [25], was used for the generation of deletion strains. SIJ488 carries the gene deletion machinery in its genome (inducible recombinase and flippase). All gene deletions were carried out by successive rounds of λ-Red recombineering [25] using kanamycin cassettes (Gene Bridges, Heidelberg, Germany) with homologous extensions generated by PCR using primers listed in Table 2.

For the overexpression of the glycerol dehydrogenase (*gldA*) and fructose 6-phosphate aldolase (*fsaA*) the corresponding genes were amplified from *E. coli* genomic DNA by a two-step PCR (to remove cloning system relevant restriction sites [26]) using in the first PCR primer pairs gldA_A + gldA_B, gldA_C + gldA_D as well as fsaA_A + fsaA_B, fsaA_C + fsaA_D. The corresponding PCR products where fused in a second PCR using primer pairs gldA_A + gldA_D and fsaA_A + fsaA_D respectively. Amplified *gldA* and *fsaA* genes were cloned into cloning vector pNivC using restriction enzymes *Nsi*I and *Nhe*I, generating pNivC-gldA and pNivC-fsaA. To generate pNiv-gldA-fsaA, fsaA was cut from pNivC-fsaA with *Spe*I and *Sal*I and cloned into *Nhe*I and *Xho*I cut pNivC-gldA. gldA-fsaA was cloned from pNiv-gldA-fsaA into expression vector pZ-ASS using enzymes *Eco*RI and *Pst*I, resulting in pZ-ASS-gldA-fsaA [26].

Cultivation conditions

For strain maintenance, generation of deletion strains, and for growth during cloning we used LB medium (1% NaCl, 0.5% yeast extract, 1% tryptone). For selection, antibiotics were used in following concentrations: kanamycin, 25 μg·mL^{-1}; ampicillin, 100 μg·mL^{-1}; streptomycin, 100 μg·mL^{-1}. M9 minimal media were used for growth experiments (50 mM Na$_2$HPO$_4$, 20 mM KH$_2$PO$_4$, 1 mM NaCl, 20 mM NH$_4$Cl, 2 mM MgSO$_4$ and 100 μM CaCl$_2$, 134 μM EDTA, 13 μM FeCl$_3$·6H$_2$O, 6.2 μM ZnCl$_2$, 0.76 μM CuCl$_2$·2H$_2$O, 0.42 μM CoCl$_2$·2H$_2$O, 1.62 μM H$_3$BO$_3$, 0.081 μM MnCl$_2$·4H$_2$O).

For growth experiments over-night cultures were incubated in 4 mL M9 medium containing 10 mM glucose. Before inoculation of the experiment, cultures were harvested and washed three times in M9 medium without carbon source by centrifugation (4000 *g*, 3 min) to wash away residual carbon sources. For plate reader and tube experiments cultures were inoculated with a starting OD$_{600}$ of 0.01. Plate reader experiments were carried out in 96-well microtitre plates (Nunclon Delta Surface; Thermo Scientific, Waltham, MA, USA) at 37 °C. Each well contained 150 μL of cell culture covered by 50 μL mineral oil (Merck KGaA, Darmstadt, Germany), to avoid evaporation. Infinite M200 pro plate reader (Tecan, Männedorf, Switzerland) was used for incubation, shaking and OD$_{600}$ measurements. Three cycles of 4 shaking phases, each of 1 min were run [(a) linear shaking at an amplitude of 3 mm, (b) orbital shaking at an amplitude of 3 mm, (c) linear shaking at an amplitude of 2 mm, and (d) orbital shaking at an amplitude of 2 mm]. Optical density (OD 600 nm) was measured after each round of shaking (~ 12.5 min). Plate reader OD measurements were converted to cuvette values according to OD$_{cuvette}$ = OD$_{plate}$/0.23. Growth curves were plotted in MATLAB (MathWorks, Natick, MA, USA) and represent averages of triplicate measurements; in all cases, variability between triplicate measurements was < 10%.

Table 1. Strains and plasmids used in this study

Name	Description/gene deletions	Reference
DH5α	Cloning of overexpression constructs	
SIJ488	WT	[25]
ΔglpK ΔdhaK	Strain deficient in glycerol assimilation pathways: deletion of the glycerol kinase gene *glpK* and subunit of dihydroxyacetone kinase gene *dhaK*	This study
ΔglpK ΔdhaK Δfbp ΔglpX	Strain deficient in glycerol assimilation pathways (see above) and fructose 1,6-bisphosphatases (encoded by *fbp* and *glpX*) necessary for growth on gluconegentic carbon sources	This study
ΔglpK ΔdhaK ΔpfkA ΔpfkB	Strain deficient in glycerol assimilation pathways (see above) and 6-phosphofructokinases (encoded by *pfkA* and *pfkB*)	This study
ΔglpK ΔdhaK Δzwf	Strain deficient in glycerol assimilation pathways (see above) and glucose 6-phosphate dehydrogenase (encoded by *zwf*)	This study
pZ-ASS	Overexpression plasmid with p15A origin, Streptomycin resistance, constitutive strong promoter (5′-AATACTTGACATATCACTGTGATTCACATATAATATGCG-3′)	[26]
pZ-ASS-gldA-fsaA	pZ-ASS backbone for overexpression of *Escherichia coli gldA* (coding for glycerol dehydrogenase) and *fsaA* (encoding fructose 6-phosphate aldolase)	This study
pZ-ASS-gldA	pZ-ASS backbone for overexpression of *E. coli gldA* (encoding glycerol dehydrogenase)	This study
pZ-ASS-fsaA	pZ-ASS backbone for overexpression of *E. coli fsaA* (encoding fructose 6-phosphate aldolase)	This study

Chemostat cultivation

The Δ*glpK* Δ*dhaK* pZ-ASS-*gldA-fsaA* was incubated under chemostat conditions in an Eppendorf DASGIP Parallel Bioreactor, composed of bioblock, MX4/4 Gassing System, MP8 Multipump Modules, TCSC Temperature and Stirrer Control System, OD4 Optical Density Module controlled by DASWARE CONTROL 5 software (Eppendorf AG, Jülich, Germany). Initial inoculation resulted in an OD of 0.05 into 300 mL of MS medium (50 mM K_2HPO_4, 20 mM NH_4Cl, 4 mM citrate, 1 mM $MgSO_4$, 3 μM $FeCl_3$, 1 μM $MnCl_2$, 1 μM $CaCl_2$ [27]) containing 50 mM glycerol, 5 mM sodium pyruvate and 100 μg·mL^{-1} Streptomycin. The bioreactor was equipped with Rushton-type-impeller, an L-sparger for gasing, pH probe, sensor for dissolved oxygen (DO), OD metre and off-gas condenser. The temperature was set to 37 °C and flow rate of air for gasing according to DO sensor to maintain 95% DO. After 2 days of cultivation in batch mode conditions were changed to chemostat. An inflow rate of fresh medium of 8.66 mL·h^{-1} was set according to an estimated doubling time of 24 h. Seven days after inoculation flow rate of fresh medium was changed to 11.55 mL·h^{-1} giving a doubling time of 18 h, which remained till the end of the cultivation. Seventy-five days after cultivation at a stable OD (600 nm) of 0.295, sodium pyruvate concentration was reduced from 5 to 3 mM.

Batch cultivation in bioreactor

Precultures for the bioreactor cultivations of *E. coli* Δ*glpK* Δ*dhaK* pZ-ASS-*gldA-fsaA* were prepared by thawing a glycerol stock (30% w/v glycerol) and streaking cell solution on a 2×YT [28] agar plate which was incubated at 37 °C for 24 h. A single colony was used to inoculate 5 mL 2×YT complex medium in a glass test tube, which was incubated at 37 °C on a rotary shaker at 120 r.p.m. for 7 h. The suspension was then used to inoculate 50 mL of M9 minimal medium with 10 mM glucose in a 500 mL baffled shaking flask to an optical density at 600 nm (OD_{600}) of 0.1, which was incubated at 37 °C on a rotary shaker at 120 r.p.m. overnight. To inoculate the main culture in the bioreactor, cells were harvested by centrifugation (4500 *g*, 10 min, 4 °C), the pellet was resuspended in 0.9% w/v NaCl solution and used to inoculate M9 minimal medium with 500 mM glycerol to an OD_{600} of 0.2. All cultures contained 100 μg streptomycin·mL^{-1}. The aerobic bioreactor cultivations of *E. coli* Δ*glpK* Δ*dhaK* pZ-ASS-*gldA-fsaA* were performed at 37 °C as 200 mL cultures in glass vessels. The pH was maintained at 7.0 by online measurement using a standard pH probe (Mettler Toledo, Giessen, Germany) and addition of 12.5% NH_4OH and 10% H_3PO_4. DO was measured online using a polarometric oxygen electrode (Mettler Toledo) and adjusted to ≥ 30% of saturation by stirring at 300 r.p.m. with aeration at 0.25 volume per volume per minute. Three independent cultivations were performed.

Detection of extracellular compounds

To analyse the presence of secreted products in the culture fluid of the bioreactor, 2 mL of the culture was harvested by centrifugation (12 100 *g*, 5 min, RT) at the given time points. The supernatant was analysed by HPLC using an Agilent 1200 Series apparatus (Agilent, Santa Clara, CA, USA) with a refractive index detector equipped with a Rezex ROA organic acid column H$^+$ (8%) column (300 × 7.8 mm, 8 μm; Phenomenex, Torrance, CA, USA), protected by a Phenomenex security guard column carbo-H (4 × 3.0 mm ID) (Phenomenex, Torrance, CA, USA) as described in Ref. [29]. Dihydroxyacetone concentrations in

Table 2. Oligonucleotide primers used. Primers containing 'KO' in their name were used to amplify knockout the cassette FRT-PGK-gb2-neo-FRT (Gene Bridges; binding sequences are highlighted in bold) with 50 bp gene-specific upstream and downstream of the target sequences. Primers containing 'KO-Ver' (knockout-verification) were used in PCRs to verify the gene deletion by kanamycin resistance cassette integration and subsequent kanamycin-cassette removal by flippase

Name	Sequence (5′ → 3′)
gldA_A	ATGCATCATCACCATCACCACGACCGCATTATTCAATCACCGGGTAAATACATC
gldA_B	CGACGATTTTGGTATCGACAATGACCATATTC
gldA_C	GAATATGGTCATTGTCGATACCAAAATCGTCG
gldA_D	CTCTTACGTGCCCGATCAACGCTAGCTTATTCCCACTCTTGCAGGAAACGCTGAC
fsaA_A	CTTTAAAGTTAAGAGGCAAGAATGCATCATCACCATCACCACGAACTGTATCTGGATACTTCAGACGTTG TTGCG
fsaA_B	CGCCTGCGGCGCGTGCATTTTCAATAACTG
fsaA_C	CAGTTATTGAAAATGCACGCGCCGCAGGCG
fsaA_D	CTCTTACGTGCCCGATCAACGCTAGCTTAAATCGACGTTCTGCCAAACGCTCCCTG
glpK_KO_F	TTCAGAACAAAAAGCTTCGCTGTAATATGACTACGGGACAATTAAACATG**AATTAACCCTCACTAAAGGGCG**
glpK_KO_R	CGGCATAAACGCTTCATTCGGCATTTACATTATTCGTCGTGTTCTTCCCA**TAATACGACTCACTATAGGGCTC**
glpK_KO_V_F	GACGCGGGAAAATTCGATGG
glpK_KO_V_R	GCGCGATTGTAGGTGCATTT
dhaK_KO_F	GAGTTCTGCTCAGTGACATTGCTTTCTCCTTATTTACCCCAGTTAAGGGC**AATTAACCCTCACTAAAGGGCG**
dhaK_KO_R	ATGGATTCATCGGCAGTCAGTGGTCGCCGTGTCGTTGAACATCATCCATG**TAATACGACTCACTATAGGGCTC**
dhaK_KO_V_F	GCCAATTTCGCGATCCAGTC
dhaK_KO_V_R	CAGCATCGCTTTCTTACGCC
fbp_KO_F	AAAAACGCCTCTCCGTGTGGAGAGGCGCAGGAGATTACGCGTCCGGGAAC**ATTAACCCTCACTAAAGGGCG**
fbp_KO_R	CTTTACTCCATAAACATTGCAGGGAAAGTTTTATGAAAACGTTAGGTGAA**TAATACGACTCACTATAGGGCTC**
fbp_KO_Ver_F	AGTGGTAATTGGCGGTACGC
fbp_KO_Ver_R	AGGTGCTCATCGGCGGATAC
glpX_KO_F	GGACTGGAAGGCTCAATCGATCAAATCAATCAGAGGATGTGCACCTGCAT**ATTAACCCTCACTAAAGGGCG**
glpX_KO_R	CTTCGCGCCATTCCTTACTGCTTAGAGTTTGCTATGAGACGAGAACTTGC**TAATACGACTCACTATAGGGCTC**
glpX_KO_Ver_F	GAAACCACTGAGCGTAATTA
glpX_KO_Ver_R	GTTCGCCGTCGATTTCAAGG

supernatants of the bioreactor or from tube experiments were determined enzymatically according to Ref. [30]. Glycylglycine buffer pH 9 containing 25 mM glycylglycine, 10 mM ammoniumsulphate, 10% w/v sucrose and 0.2 mM NADH was incubated with samples/standards until absorption at 340 nm was stable. The reaction was started with the addition of 2 U glycerol dehydrogenase and $\Delta Abs_{340\ nm}$ was used to determine dihydroxyacetone concentrations. Absorption changes of dihydroxyacetone standards were measured in the presence of different glycerol concentrations (according to the starting glycerol concentrations in the experiment, 17, 25, 35, 48, 68, 95, 133, 186, 260, 364, 510, 714, 1000, 1400 mM).

Determination of biomass

Cells were harvested from cultures growing in 500 mM glycerol in shake flasks. Up to 50 mL of cells was harvested by centrifugation (3220 *g*, 20 min), resuspended in 2 mL H_2O and washed three times following cycles of centrifugation (7000 *g*, 5 min) and resuspension in 2 mL H_2O. Washed cell solutions were transferred to aluminium trays, dried at 90 °C for 16 h, and weight of the dried cells was determined.

Isotopic-labelling experiments

To deduce carbon source contribution to central metabolism stationary isotope tracing of proteinogenic amino acids was performed. Strains were grown in M9 with 20 mM pyruvate and 20 mM either unlabelled or completely (triply) labelled glycerol (Merck). Experiments were performed in duplicate. One millilitre of culture per OD_{600} of 1 was harvested by centrifugation and washed twice in water. Protein biomass was hydrolysed by incubation at 95 °C in 6 M HCl for 24 h [31]. After drying the samples under an air-stream at 95 °C, they were resuspended in water and masses of amino acids were analysed with UPLC–ESI–MS as previously described [32]. Chromatography was performed with a Waters Acquity UPLC system (Waters, Eschborn, Germany), using an HSS T3 C_{18} reversed phase column (100 mm × 2.1 mm, 1.8 μm; Waters). 0.1% formic acid in H_2O (A) and 0.1% formic acid in acetonitrile (B) were the mobile phases. Flow rate was 0.4 mL·min^{-1} and the gradient was: 0–1 min – 99% A; 1–5 min – linear gradient from 99% A to 82%; 5–6 min – linear gradient from 82% A to 1% A; 6–8 min – kept at 1% A; 8–8.5 min – linear gradient to 99% A; 8.5–11 min – re-equilibrate. Mass spectra were acquired using an Exactive mass spectrometer (Thermo Scientific) in positive ionization mode,

with a scan range of 50.0–300.0 *m/z*. Spectra were recorded during the first 5 min of the LC gradients. Data analysis was performed using Xcalibur (Thermo Scientific). Determination of retention times was performed by analysing amino acid standards (Merck) under the same conditions.

Acknowledgements

Conflict of interest

The authors declare no conflict of interest.

Author contributions

SNL and AB-E conceptualized project and designed experiments. AB-E supervised the project. SNL, SA and AM constructed strains and cloned necessary genes. SNL, EH and BB performed growth experiments. EH and BB measured the accumulation of byproducts in the medium. PB performed long-term cultivation under selective conditions. CE-M and AB-E performed computational analysis. SNL and AB-E generated the figures. SNL, BB and AB-E wrote the paper.

References

1 Verhees CH, Kengen SW, Tuininga JE, Schut GJ, Adams MW, De Vos WM & Van Der Oost J (2003) The unique features of glycolytic pathways in Archaea. *Biochem J* **375**, 231–246.

2 Siebers B & Schonheit P (2005) Unusual pathways and enzymes of central carbohydrate metabolism in Archaea. *Curr Opin Microbiol* **8**, 695–705.

3 Ahmed H, Ettema TJ, Tjaden B, Geerling AC, van der Oost J & Siebers B (2005) The semi-phosphorylative Entner-Doudoroff pathway in hyperthermophilic archaea: a re-evaluation. *Biochem J* **390**, 529–540.

4 Flamholz A, Noor E, Bar-Even A, Liebermeister W & Milo R (2013) Glycolytic strategy as a tradeoff between energy yield and protein cost. *Proc Natl Acad Sci USA* **110**, 10039–10044.

5 Hopper DJ & Cooper RA (1971) The regulation of *Escherichia coli* methylglyoxal synthase; a new control site in glycolysis? *FEBS Lett* **13**, 213–216.

6 Booth IR, Ferguson GP, Miller S, Li C, Gunasekera B & Kinghorn S (2003) Bacterial production of methylglyoxal: a survival strategy or death by misadventure? *Biochem Soc Trans* **31**, 1406–1408.

7 Clark DP (1989) The fermentation pathways of *Escherichia coli*. *FEMS Microbiol Lett* **63**, 223–234.

8 Levanon SS, San KY & Bennett GN (2005) Effect of oxygen on the *Escherichia coli* ArcA and FNR regulation systems and metabolic responses. *Biotechnol Bioeng* **89**, 556–564.

9 Lin EC (1976) Glycerol dissimilation and its regulation in bacteria. *Annu Rev Microbiol* **30**, 535–578.

10 Donahue JL, Bownas JL, Niehaus WG & Larson TJ (2000) Purification and characterization of glpX-encoded fructose 1, 6-bisphosphatase, a new enzyme of the glycerol 3-phosphate regulon of *Escherichia coli*. *J Bacteriol* **182**, 5624–5627.

11 Flamholz A, Noor E, Bar-Even A & Milo R (2012) eQuilibrator–the biochemical thermodynamics calculator. *Nucleic Acids Res* **40**, D770–D775.

12 Alberty RA, Cornish-Bowden A, Goldberg RN, Hammes GG, Tipton K & Westerhoff HV (2011) Recommendations for terminology and databases for biochemical thermodynamics. *Biophys Chem* **155**, 89–103.

13 Bennett BD, Kimball EH, Gao M, Osterhout R, Van Dien SJ & Rabinowitz JD (2009) Absolute metabolite concentrations and implied enzyme active site occupancy in *Escherichia coli*. *Nat Chem Biol* **5**, 593–599.

14 Monod J (1949) The growth of bacterial cultures. *Annu Rev Microbiol* **3**, 371–394.

15 Ukeda H, Hasegawa Y, Ishi T & Sawamura M (1997) Inactivation of Cu, Zn-superoxide dismutase by intermediates of Maillard reaction and glycolytic pathway and some sugars. *Biosci Biotechnol Biochem* **61**, 2039–2042.

16 Subedi KP, Kim I, Kim J, Min B & Park C (2008) Role of GldA in dihydroxyacetone and methylglyoxal metabolism of *Escherichia coli* K12. *FEMS Microbiol Lett* **279**, 180–187.

17 Molin M, Pilon M & Blomberg A (2007) Dihydroxyacetone-induced death is accompanied by advanced glycation endproduct formation in selected proteins of *Saccharomyces cerevisiae* and *Caenorhabditis elegans*. *Proteomics* **7**, 3764–3774.

18 Kovarova-Kovar K & Egli T (1998) Growth kinetics of suspended microbial cells: from single-substrate-controlled growth to mixed-substrate kinetics. *Microbiol Mol Biol Rev* **62**, 646–666.

19 Liu Y (2007) Overview of some theoretical approaches for derivation of the Monod equation. *Appl Microbiol Biotechnol* **73**, 1241–1250.

20 Noor E, Flamholz A, Liebermeister W, Bar-Even A & Milo R (2013) A note on the kinetics of enzyme action: a decomposition that highlights thermodynamic effects. *FEBS Lett* **587**, 2772–2777.

21 Noor E, Bar-Even A, Flamholz A, Reznik E, Liebermeister W & Milo R (2014) Pathway thermodynamics highlights kinetic obstacles in central metabolism. *PLoS Comput Biol* **10**, e1003483.

22 Cleland WW (1982) An analysis of Haldane relationships. *Methods Enzymol* **87**, 366–369.

23 Sprenger GA, Schorken U, Sprenger G & Sahm H (1995) Transketolase A of *Escherichia coli* K12. Purification and properties of the enzyme from recombinant strains. *Eur J Biochem* **230**, 525–532.

24 Lloyd RV, Fong AJ & Sayre RM (2001) In vivo formation of Maillard reaction free radicals in mouse skin. *J Invest Dermatol* **117**, 740–742.

25 Jensen SI, Lennen RM, Herrgard MJ & Nielsen AT (2015) Seven gene deletions in seven days: fast generation of *Escherichia coli* strains tolerant to acetate and osmotic stress. *Sci Rep* **5**, 17874.

26 Wenk S, Yishai O, Lindner SN & Bar-Even A (2018) An engineering approach for rewiring microbial metabolism. *Methods Enzymol* **608**, 329–367.

27 Richaud C, Mengin-Lecreulx D, Pochet S, Johnson EJ, Cohen GN & Marliere P (1993) Directed evolution of biosynthetic pathways. Recruitment of cysteine thioethers for constructing the cell wall of *Escherichia coli*. *J Biol Chem* **268**, 26827–26835.

28 Sambrook J & Russell DW (2001) Molecular Cloning: A Laboratory Manual, 3rd edn. Cold Spring Harbor Laboratory Press, Cold Spring Harbor, NY.

29 Hoffart E, Grenz S, Lange J, Nitschel R, Müller F, Schwentner A, Feith A, Lenfers-Lucker M, Takors R & Blombach B (2017) High substrate uptake rates empower *Vibrio natriegens* as production host for industrial biotechnology. *Appl Environ Microbiol* **83**, e01614–e01617.

30 Sponholz W-R & Wünsch B (1980) Enzymatische bestimmung von dihydroxyaceton in Gegenwart von glycerin. *Z Lebensm Unters Forsch* **171**, 178–197.

31 You L, Page L, Feng X, Berla B, Pakrasi HB & Tang YJ (2012) Metabolic pathway confirmation and discovery through 13C-labeling of proteinogenic amino acids. *J Vis Exp* **59**, e3583.

32 Giavalisco P, Li Y, Matthes A, Eckhardt A, Hubberten HM, Hesse H, Segu S, Hummel J, Köhl K & Willmitzer L (2011) Elemental formula annotation of polar and lipophilic metabolites using 13C, 15N and 34S isotope labelling, in combination with high-resolution mass spectrometry. *Plant J* **68**, 364–376.

33 Bar-Even A, Noor E, Flamholz A, Buescher JM & Milo R (2011) Hydrophobicity and charge shape cellular metabolite concentrations. *PLoS Comput Biol* **7**, e1002166.